PUBLISHED SUPPLEMENTAL MATERIAL

NMR in Biomedicine – 2020

Hypertension – 2019

Scientific Reports - 2019

– SUPPLEMENTAL MATERIAL –

Longitudinal Assessment of Tissue Properties and Cardiac Diffusion Metrics of the Ex-vivo Porcine Heart at 7T: Impact of Progressive Tissue Fixation Using Formalin

Running Head: Influence of Tissue Fixation on Cardiac Diffusion Tensor Imaging

David Lohr[1]*, Maxim Terekhov[1], Franziska Veit[2], Laura Maria Schreiber[1]

[1]Chair of Cellular and Molecular Imaging, Comprehensive Heart Failure Center (CHFC), University Hospital Wuerzburg, Wuerzburg, Germany

[2]Chair Tissue Engineering and Regenerative Medicine (TERM), University Hospital Wuerzburg, Wuerzburg, Germany

*Correspondence
David Lohr, MSc
Chair of Cellular and Molecular Imaging
Comprehensive Heart Failure Center (CHFC)
University Hospital Wuerzburg
Am Schwarzenberg 15
97078 Wuerzburg
Germany
Phone: +49 30 450 525 002
E-Mail: e_lohr_d@ukw.de

Supplemental Tables

Table S1: Information on age and weight of the study animals.

Animal #	Age [days]	Weight [kg]
1	71	21.5
2	71	21.5
3	64	20.0
4	79	21.0
5	78	21.0
6	91	21.0
7	73	22.0
8	62	22.0
Mean	73	21.3

Table S2: *P*-values of paired t-test prior Bonferroni correction for T_2 and T_2^* values. **Non-significant** values post Bonferroni correction are marked in red.

Group	***P* (T_2)**			***P* (T_2^*)**		
	Basal	**Mid-cavity**	**Apical**	**Basal**	**Mid-cavity**	**Apical**
d0 – d7	$2.2*10^{-8}$	$3.6*10^{-8}$	$3.9*10^{-6}$	$9.0*10^{-7}$	$3.0*10^{-5}$	$1.3*10^{-5}$
d0 – d15	$6.6*10^{-9}$	$1.2*10^{-7}$	$5.9*10^{-6}$	$3.4*10^{-4}$	$1.2*10^{-4}$	$3.1*10^{-5}$
d0 – d50	$6.0*10^{-6}$	$3.5*10^{-6}$	$4.4*10^{-5}$	$3.3*10^{-3}$	$6.6*10^{-1}$	$8.9*10^{-2}$
d0 – d100	$6.4*10^{-8}$	$1.7*10^{-6}$	$2.8*10^{-5}$	$1.0*10^{-1}$	$8.3*10^{-1}$	$5.9*10^{-3}$
d0 – d200	$1.8*10^{-7}$	$1.4*10^{-6}$	$5.5*10^{-5}$	$9.4*10^{-1}$	$2.3*10^{-2}$	$1.7*10^{-1}$
d7 – d15	$6.3*10^{-1}$	$6.5*10^{-3}$	$6.5*10^{-3}$	$7.4*10^{-2}$	$2.6*10^{-1}$	$3.0*10^{-1}$
d7 – d50	$6.5*10^{-4}$	$2.5*10^{-1}$	$3.1*10^{-1}$	$2.1*10^{-3}$	$2.0*10^{-2}$	$6.0*10^{-2}$
d7 – d100	$5.5*10^{-7}$	$5.2*10^{-3}$	$2.2*10^{-2}$	$4.9*10^{-5}$	$5.7*10^{-6}$	$4.5*10^{-4}$
d7 – d200	$1.5*10^{-6}$	$2.3*10^{-5}$	$1.3*10^{-4}$	$6.9*10^{-7}$	$7.5*10^{-10}$	$7.3*10^{-6}$
d15 – d50	$1.6*10^{-3}$	$1.2*10^{-3}$	$6.0*10^{-4}$	$3.6*10^{-2}$	$1.1*10^{-2}$	$1.5*10^{-2}$
d15 – d100	$4.6*10^{-6}$	$1.6*10^{-5}$	$4.9*10^{-5}$	$3.7*10^{-4}$	$3.7*10^{-6}$	$6.5*10^{-5}$
d15 – d200	$1.1*10^{-5}$	$5.3*10^{-8}$	$3.7*10^{-8}$	$1.2*10^{-4}$	$7.7*10^{-8}$	$1.8*10^{-6}$
d50 – d100	$7.0*10^{-1}$	$4.0*10^{-3}$	$6.3*10^{-2}$	$1.7*10^{-2}$	$6.2*10^{-1}$	$9.9*10^{-1}$
d50 – d200	$6.3*10^{-1}$	$4.5*10^{-4}$	$1.6*10^{-3}$	$5.7*10^{-3}$	$1.2*10^{-1}$	$1.4*10^{-1}$
d100 – d200	$7.2*10^{-1}$	$1.1*10^{-2}$	$5.8*10^{-2}$	$5.7*10^{-2}$	$2.6*10^{-3}$	$1.0*10^{-3}$

Supplemental Figures

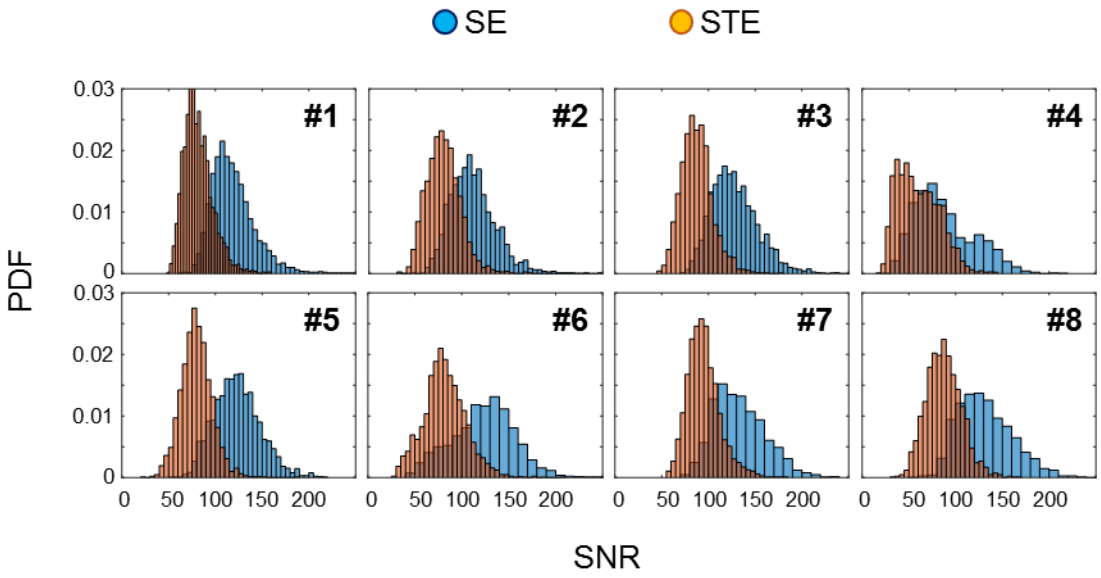

Figure S1: SNR distribution in reference scans of the spin echo and stimulated echo (t_{Mix}=100ms) sequence for all hearts.

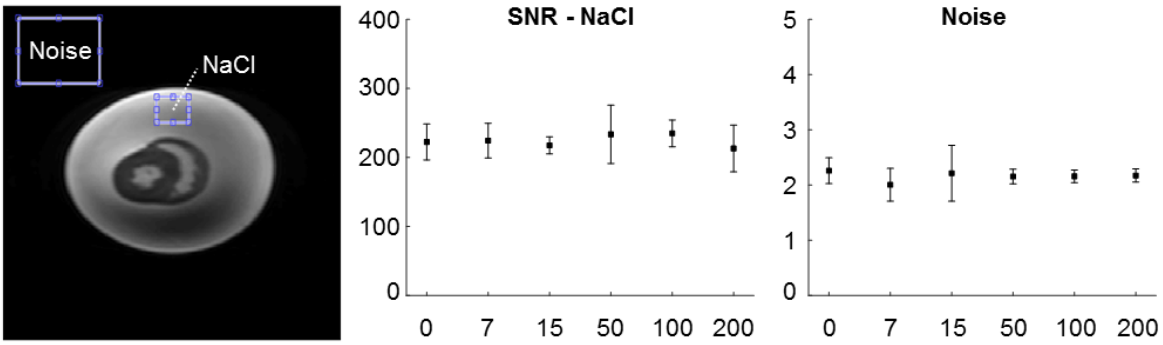

Figure S2: Reference data for SNR evaluation. Left: Representative placement of ROIs for the SNR in the saline solution and the background noise. Middle: Mean SNR ± single standard deviation in saline solution for measurements of the eight hearts at 0, 7, 15, 50, 100, and 200 days after fixation. Right: Respective evaluation of the noise floor.

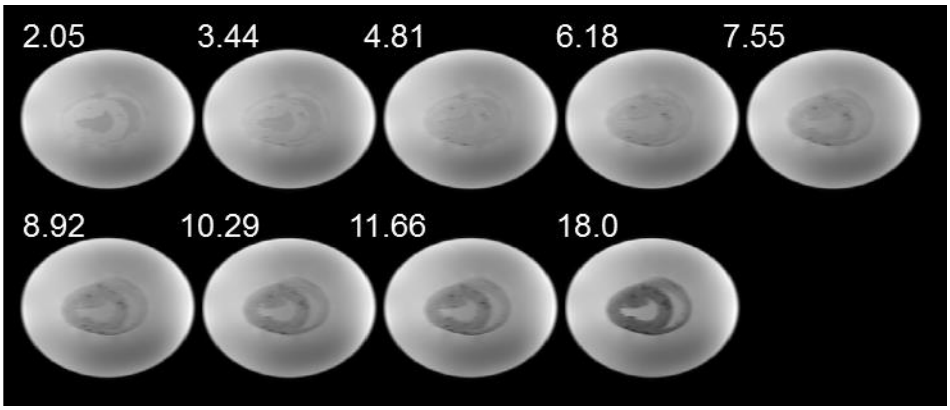

Figure S3: Representative signal evolution in a mid-cavity slice for the 9 echo times (2.07 - 18 ms) used for T_2^* estimation.

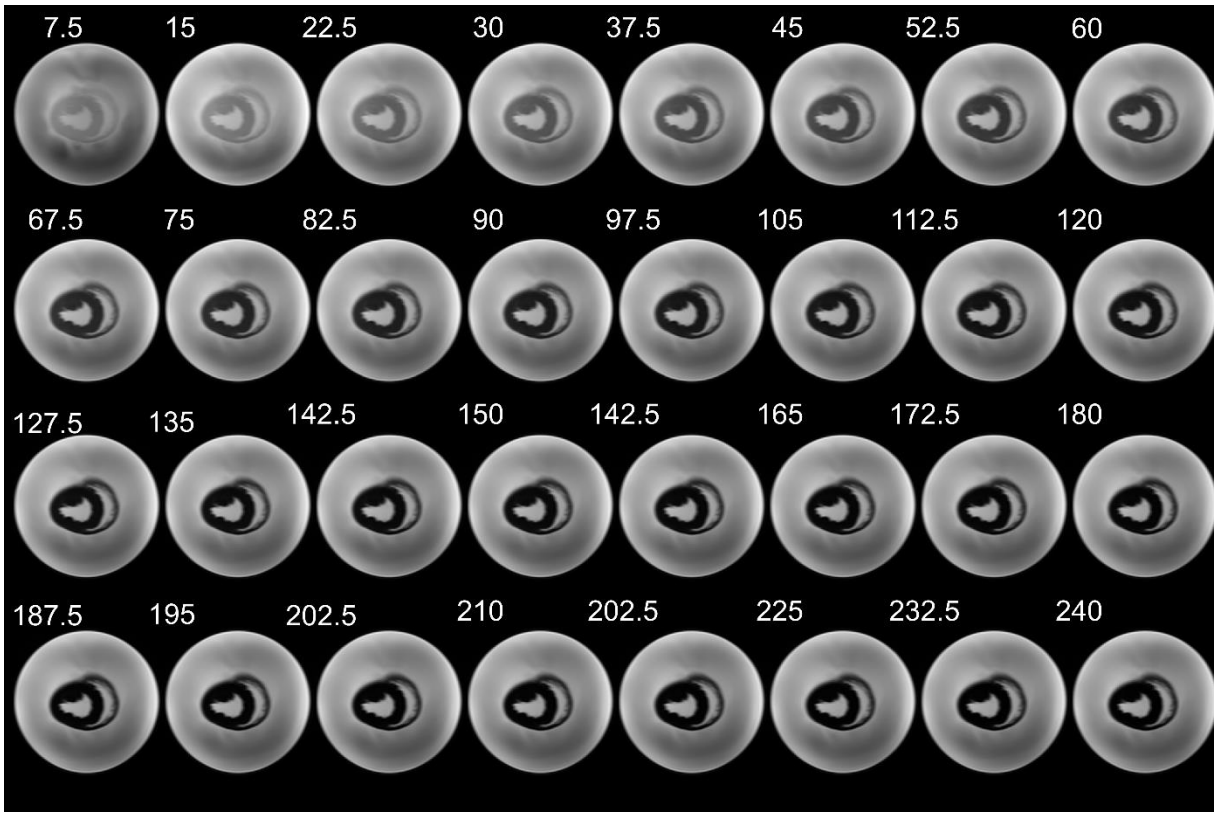

Figure S4: Representative signal evolution in a mid-cavity slice for the 32 images (TE = 7.5 : 7.5 : 240 ms) used for T_2 estimation.

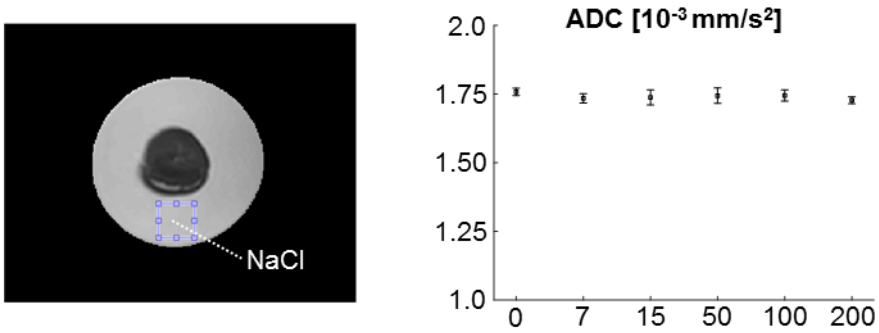

Figure S5: ADC in saline solution as a reference for DTI metrics of the LV. Left: Representative placement of ROIs in saline solution. Right: Mean ADC ± single standard deviation for the eight hearts measured 0, 7, 15, 50, 100, and 200 days after fixation.

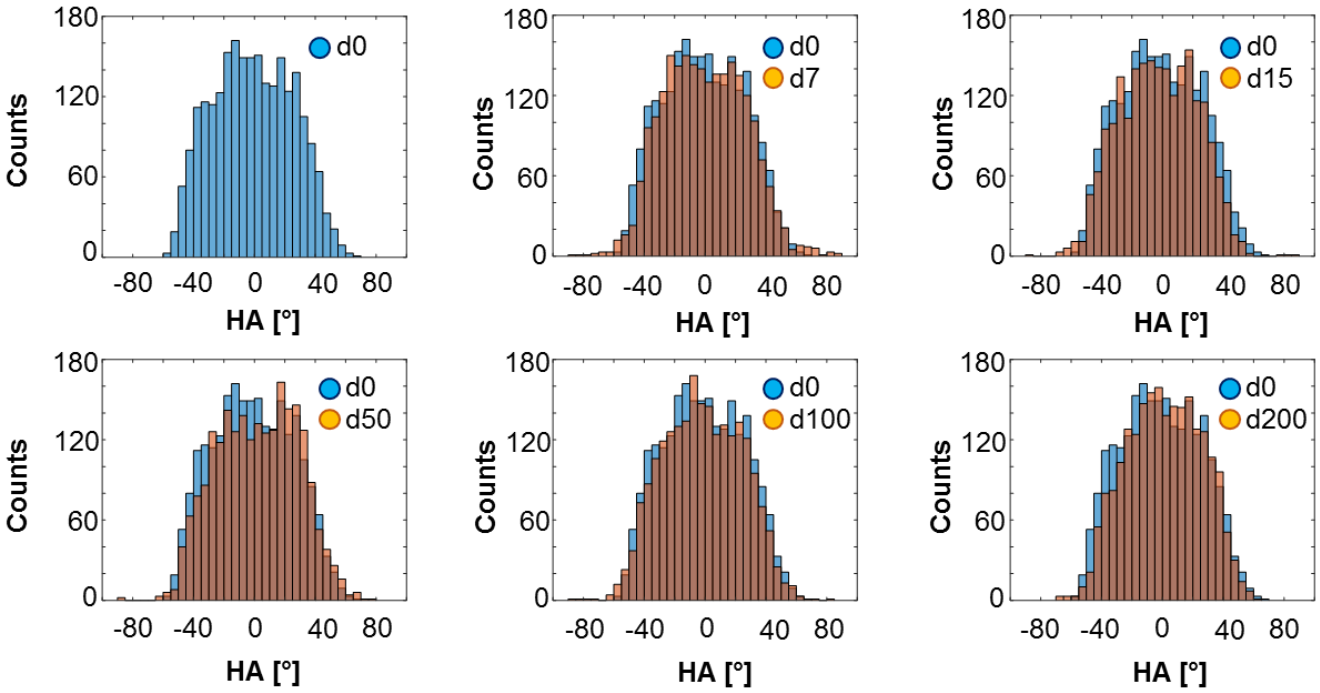

Figure S6: Representative helix angle distribution in the left ventricle of one heart prior to fixation and 7, 15, 50, 100, and 200 days after fixation. The basal slice of the respective heart is displayed in figure 5.

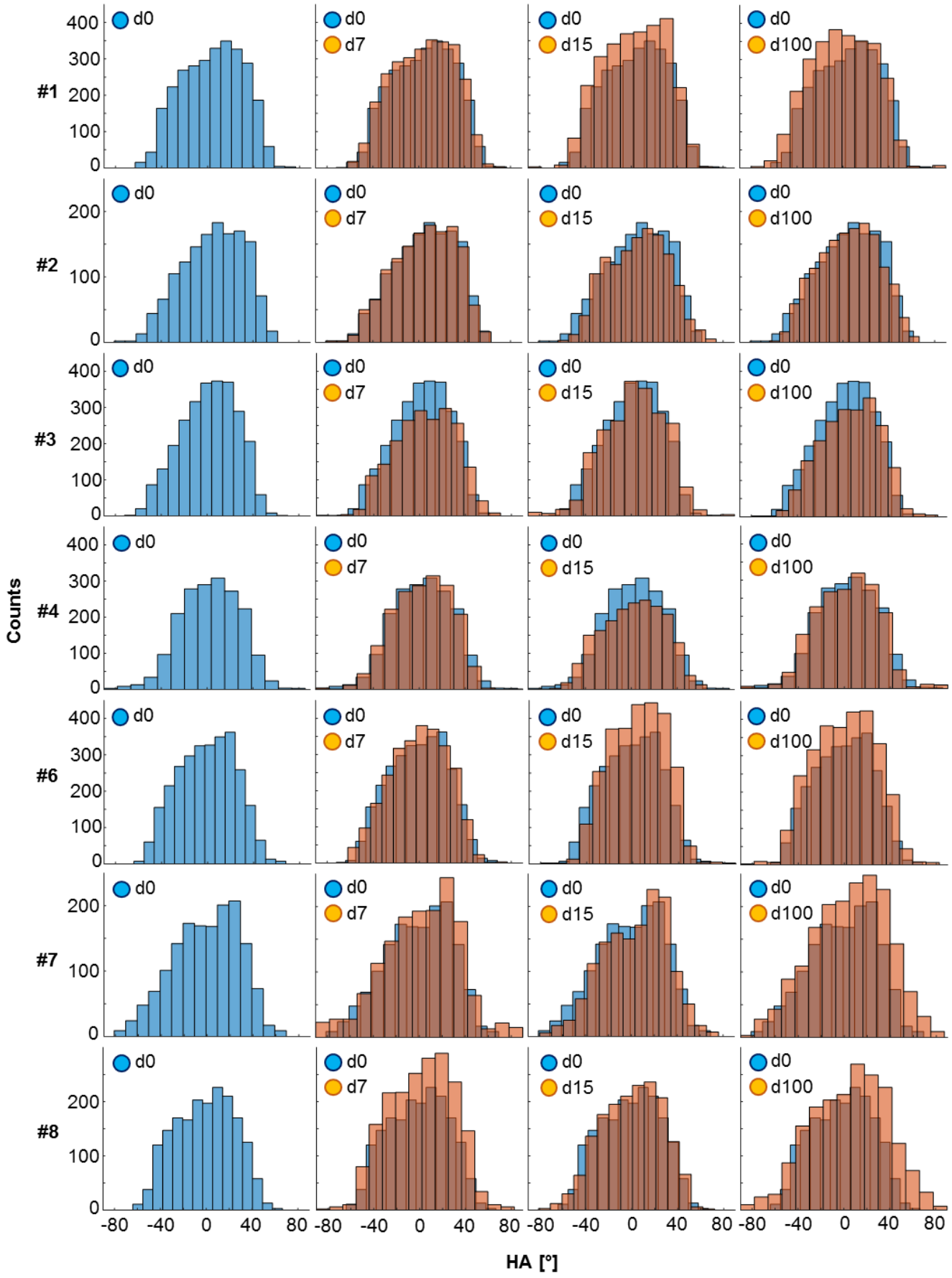

Figure S7: Helix angle distribution in the left ventricle prior to fixation and 7, 15, and 100 days after fixation.

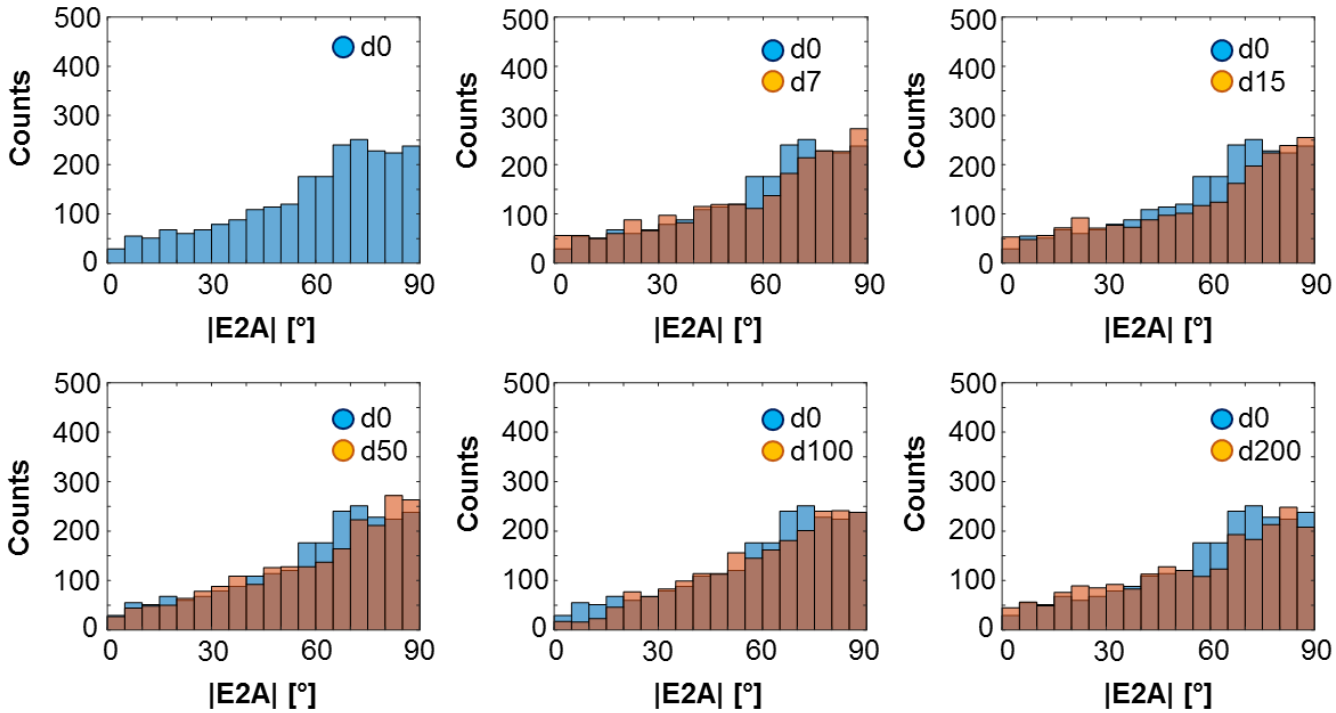

Figure S8: Representative secondary eigenvector angle distribution in the left ventricle of one heart prior to fixation and 7, 15, 50, 100, and 200 days after fixation. The basal slice of the respective heart is displayed in figure 6.

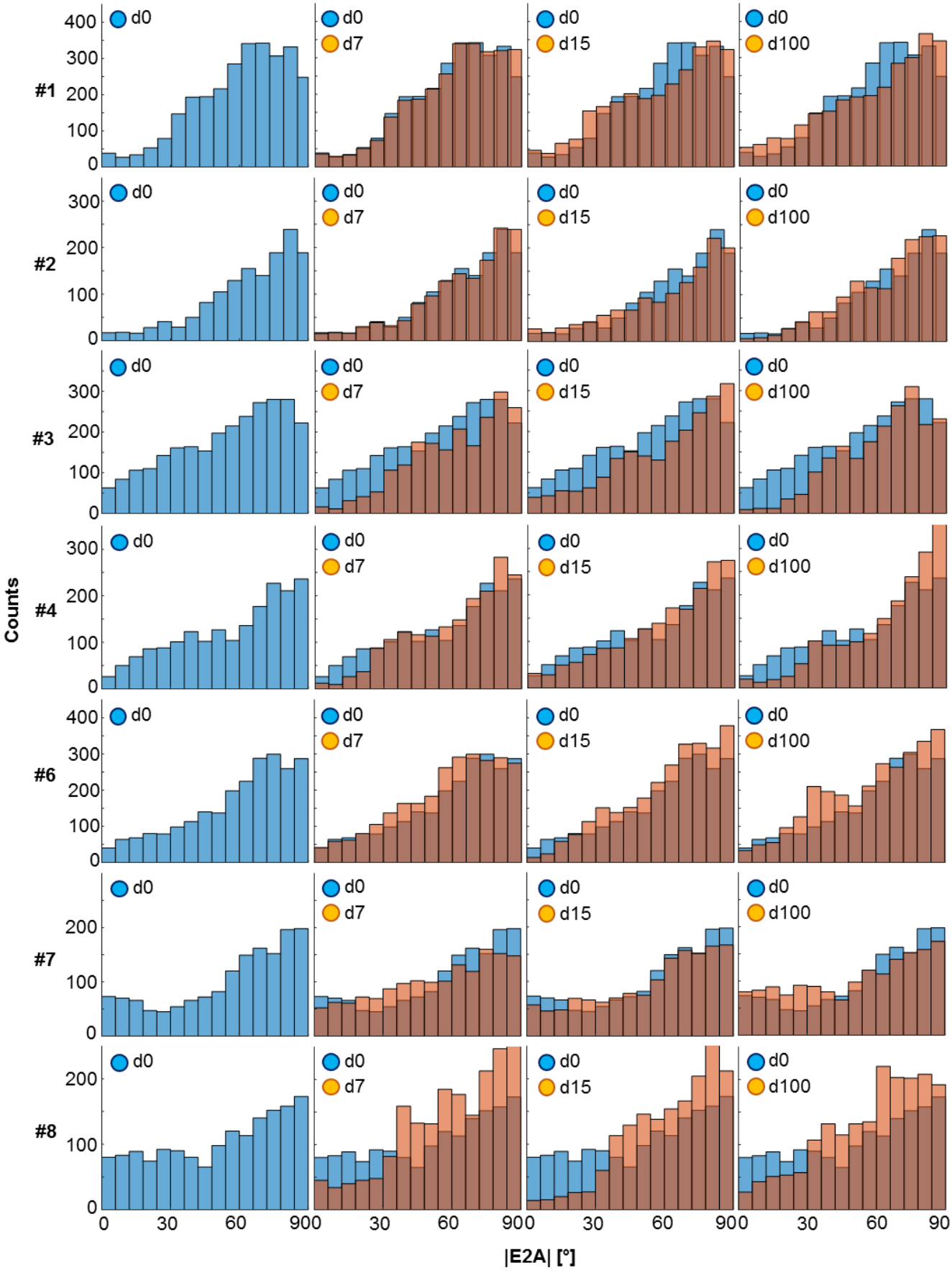

Figure S9: Secondary eigenvector angle distribution in the left ventricle prior to fixation and 7, 15, and 100 days after fixation.

– SUPPLEMENTAL MATERIAL –

Characterization of Myocardial Microstructure and Function in an Experimental Model of Isolated Subendocardial Damage

Short title: Impact of Subendocardial Damage

Niklas Beyhoff[a,b], David Lohr[c], Anna Foryst-Ludwig[a,b], Robert Klopfleisch[d], Sarah Brix[a,b], Jana Grune[a,b,e], Arne Thiele[a,b], Lasti Erfinanda[b,e], Arata Tabuchi[b,e], Wolfgang M. Kuebler[b,e], Burkert Pieske[b,f], Laura M. Schreiber[c], Ulrich Kintscher[a,b]

a) Charité - Universitätsmedizin Berlin, corporate member of Freie Universität Berlin, Humboldt-Universität zu Berlin, and Berlin Institute of Health, Institute of Pharmacology, Center for Cardiovascular Research, Berlin, Germany
b) DZHK (German Centre for Cardiovascular Research), Partner site Berlin, Berlin, Germany
c) Chair of Cellular and Molecular Imaging, Comprehensive Heart Failure Center (CHFC), University Hospital Wuerzburg, Wuerzburg, Germany
d) Department of Veterinary Pathology, College of Veterinary Medicine, Freie Universitaet Berlin, Berlin, Germany
e) Charité - Universitätsmedizin Berlin, corporate member of Freie Universität Berlin, Humboldt-Universität zu Berlin, and Berlin Institute of Health, Institute of Physiology, Berlin, Germany
f) Department of Internal Medicine and Cardiology, Campus Virchow Klinikum, Charité - Universitätsmedizin Berlin and Deutsches Herzzentrum Berlin (DHZB), Department of Cardiology, Berlin, German

Correspondence
Prof. Ulrich Kintscher, MD
Institute of Pharmacology
Center for Cardiovascular Research
Charité - Universitaetsmedizin Berlin
Hessische Str. 3-4
10115 Berlin
Germany
Phone: +49 30 450 525 002
Fax: +49 30 450 525 901
E-Mail: ulrich.kintscher@charite.de

Supplemental Methods

Graded exercise test
Exercise capacity was determined 5-6 days after final treatment with ISO/saline by a graded exercise test protocol for mice as described before[1]. Briefly, the animals were placed in a treadmill (TSE systems, Germany) with staged increases in running speed and inclination angle (**Table S1: Graded exercise test protocol**). The end of the experiment was reached after continuous contact of the animal to the treadmill's back for more than 5 seconds (defined as point of exhaustion).

Echocardiography
Echocardiographic examinations were performed 12-13 days after final treatment with ISO/saline using a Vevo 3100 Imaging System equipped with a 30 MHz linear frequency transducer (MX400; both FUJIFILM VisualSonics, Canada). Mice were anesthetized with isoflurane (in 80% oxygen) and placed in supine position on a heated examination table (37°C) with integrated ECG electrodes. Isoflurane concentration was adjusted to 0.5-1.5% warranting comparable heart rates during the examination. All animals were scanned in the parasternal long- and short axis views as well as in the apical four chamber view according to a standard operating protocol. Reported heart rates were assessed during the echocardiographic examinations by ECG recording. Acquired images were analyzed offline using dedicated software packages (VevoLAB and VevoStrain, both FUJIFILM VisualSonics) without knowledge of histology or imaging results.
Volumetric measures were extrapolated from end-systolic and end-diastolic area traced in the parasternal long axis view. Fractional shortening was assessed in M-Mode images of the parasternal short axis view at mid-papillary level. Reported tissue velocities were measured in the apical four chamber view at the septal mitral annulus. Transmitral flow patterns were recorded in the apical four chamber view by pulsed-wave Doppler after guidance with color-Doppler.
Myocardial deformation was analyzed by speckle-tracking echocardiography as described previously[2]. Parameters of longitudinal deformation were assessed in the parasternal long axis view, in which the endocardial and epicardial borders were traced beginning at mid-basal level. Radial and circumferential deformation were determined in the parasternal short axis view, in which papillary muscles were excluded from tracing. Global peak systolic strain and strain rate values were derived from corresponding averaged segmental curves.
After completion of echocardiographic examination at rest, animals received an intraperitoneal injection of 1.5 µg/g body weight dobutamine (Sigma Aldrich, Germany), and assessment of cardiac function was repeated.

Tissue processing
Prior to euthanasia, mice received an intraperitoneal injection of heparin (500 IU; Ratiopharm, Germany) to prevent clot formation. Hearts were excised, and a 30-Gauge cannula was advanced into the aorta for retrograde perfusion with cardioplegic solution (20 mM potassium chloride). Subsequently, hearts were perfusion-fixed and stored in 4% formalin. Samples harvested for gene expression analyses were stored in liquid nitrogen without previous cardioplegic arrest. The right upper lobe of the lung was excised, and the ratio of wet-over-dry weight was determined.

DT-MRI
After perfusion fixation, formalin-fixed hearts were sent to the MRI site (Comprehensive Heart Failure Center, University Hospital Wuerzburg, Germany). There, hearts were placed in Fomblin™ (Solvay Specialty Polymers, Italy) for MRI measurements in order to adjust the RX-

chain to the tissue signal and to eliminate susceptibility artefacts at myocardial tissue-water interfaces. Afterwards, hearts were rinsed using physiological saline solution and placed in formalin again. The total storage times in formalin at the time of measurement were 75±8 and 77±6 days, respectively (p=0.84). All MRI acquisitions were performed at room temperature (~20°C) on a PharmaScan™ 70/16 7T MRI system with a Paravision 6.01 interface using a TX/2RX ^{1}H-cryoprobe (all Bruker BioSpin, Germany). High-resolution DT-MRI was performed with a spatial resolution of 100×100×100 μm^3 using a standard spin echo readout sequence with monopolar diffusion encoding[3]. A maximum b-value of 823 s/mm^2 was used by a 2.5 ms diffusion gradient and a diffusion time of 8.4 ms. The b-value includes imaging gradients and cross-terms of imaging and diffusion gradients. Two reference (b=0 s/mm^2) images were acquired and the diffusion induced signal attenuation measured along 12 directions. Imaging parameters were as follows: echo time 17.5 ms, repetition time 4000 ms, field of view 10×10 mm^2, and matrix size=100×100, number of slices=70. Total measurement time for the 8 averages was 9 hours and 20 minutes.

Processing of the diffusion data was done using in-house developed MATLAB code (MathWorks, United States) and DSI Studio (http://dsi-studio.labsolver.org, accessed April 22, 2016) in a blinded manner. Images were corrected for motion, denoised using overcomplete local partial component analysis[4], and segmentation performed according to the 17-segment model of the American Heart Association[5]. The LV volume was equally distributed into the segments “base”, “mid”, and “apex”, which were used for statistical analyses.

Helix angle values were calculated following the scheme in **Figure 3 A-B**. Fiber bundles were visualized based on a deterministic fiber tracking algorithm using DSI studio[6].

Fundamentals of DT-MRI and its application to the heart have been extensively reviewed previously[7,8].

Histologic analyses

Formalin-fixed hearts were cut at approximately 25%, 50% and 75% of the cardiac long axis (defined as apical, mid and basal portion), and sections were subsequently embedded in paraffin. Samples were stained with Picrosirius Red (Morphisto, Germany) for the detection of collagen fibers. Histologic slices were digitized at 20x magnification using an Aperio CS2 image capture device (Leica Biosystems, Germany). The subendocardial and subepicardial layer were manually defined as regions of interest, in which the red-stained collagen content was determined by a software algorithm (Aperio ImageScope and Aperio GENIE, both Leica Biosystems). Total collagen content was calculated per animal as the mean of apical, mid-myocardial and basal values.

For investigation of immune cell infiltration, longitudinal sections of the heart (n=2 per group) were stained with a rabbit polyclonal anti-CD68 antibody for the detection of macrophages (ab125212, Abcam, United Kingdom; dilution 1:1000).

Gene expression analyses

Genes of interest were selected based on recent publications[9,10], and expression levels were determined by quantitative real-time polymerase chain reaction (**Table S2: Primer pairs**).

Statistical analyses

Statistical analyses were performed with Prism 7 (GraphPad Software, United States). Data are presented as mean ± standard error of the mean. Formal power calculation was not conducted due to the explorative study design. Sample size was based on a previous study considering a mortality of 10-20% in response to ISO-treatment[2]. Differences between two groups were compared with two-tailed unpaired *Student's* t-tests. Two-way ANOVA followed by *Bonferroni's* post hoc test was used for comparisons of collagen content in different myocardial layers and treatment groups. The relationship between continuous variables was studied by

linear regression analyses. Receiver operating characteristic (ROC) curves were generated to determine sensitivity and specificity of different parameters to detect subendocardial fibrosis. Statistical significance was assumed at a p value of <0.05.

Supplemental References

1. Petrosino JM, Heiss VJ, Maurya SK, Kalyanasundaram A, Periasamy M, LaFountain RA, Wilson JM, Simonetti OP, Ziouzenkova O. Graded Maximal Exercise Testing to Assess Mouse Cardio-Metabolic Phenotypes. *PLoS One*. 2016;11:e0148010.

2. Beyhoff N, Brix S, Betz IR, Klopfleisch R, Foryst-Ludwig A, Krannich A, Stawowy P, Knebel F, Grune J, Kintscher U. Application of Speckle-Tracking Echocardiography in an Experimental Model of Isolated Subendocardial Damage. *J Am Soc Echocardiogr*. 2017;30:1239-1250.e2.

3. Abdullah OM, Drakos SG, Diakos NA, Wever-Pinzon O, Kfoury AG, Stehlik J, Selzman CH, Reid BB, Brunisholz K, Verma DR, Myrick C, Sachse FB, Li DY, Hsu EW. Characterization of Diffuse Fibrosis in the Failing Human Heart via Diffusion Tensor Imaging and Quantitative Histological Validation. *NMR Biomed*. 2014;27:1378–1386.

4. Manjón JV, Coupé P, Concha L, Buades A, Collins DL, Robles M. Diffusion Weighted Image Denoising Using Overcomplete Local PCA. *PLoS One*. 2013;8:e73021.

5. Cerqueira MD, Weissman NJ, Dilsizian V, Jacobs AK, Kaul S, Laskey WK, Pennell DJ, Rumberger JA, Ryan T, Verani MS, American Heart Association Writing Group on Myocardial Segmentation and Registration for Cardiac Imaging. Standardized myocardial segmentation and nomenclature for tomographic imaging of the heart. A statement for healthcare professionals from the Cardiac Imaging Committee of the Council on Clinical Cardiology of the American Heart Association. *Circulation*. 2002;105:539–542.

6. Yeh F-C, Verstynen TD, Wang Y, Fernández-Miranda JC, Tseng W-YI. Deterministic Diffusion Fiber Tracking Improved by Quantitative Anisotropy. *PLoS One*. 2013;8:e80713.

7. Basser PJ. Inferring microstructural features and the physiological state of tissues from diffusion-weighted images. *NMR Biomed*. 1995;8:333–344.

8. Mekkaoui C, Reese TG, Jackowski MP, Bhat H, Sosnovik DE. Diffusion MRI in the heart. *NMR Biomed*. 2017;30.

9. Ikonomidis I, Tzortzis S, Triantafyllidi H, Parissis J, Papadopoulos C, Venetsanou K, Trivilou P, Paraskevaidis I, Lekakis J. Association of impaired left ventricular twisting-untwisting with vascular dysfunction, neurohumoral activation and impaired exercise capacity in hypertensive heart disease. *Eur J Heart Fail*. 2015;17:1240–1251.

10. de Boer RA, Daniels LB, Maisel AS, Januzzi JL. State of the Art: Newer biomarkers in heart failure. *Eur J Heart Fail*. 2015;17:559–569.

Supplemental Tables

Table S1: Graded exercise test protocol. Adapted from *Petrosino et al.*[1]

Stage	Speed (m/min)	Inclination (°degree)	Duration (min)
0	0	0	3
1	6	0	2
2	9	5	2
3	12	10	2
4	15	15	2
5	18	15	1
6	21	15	1
7	23	15	1
8	24	15	1
+1	+1	15	1

Table S2: Primer pairs.

Gene	Abbreviation	Forward Primer 5'-3'	Reverse Primer 5'-3'
Atrial Natriuretic Peptide	ANP	CTGCTAGACCACCTGGAGGA	AAGCTGTTGCAGCCTAGTCC
Cluster of Differentiation 68	CD68	AATGTGTCCTTCCCACAGGC AG	AGAGCAGGTCAAGGTGAACA GC
Collagen Type I, Alpha 1 Chain	Col1a1	CTGACGCATGGCCAAGAAGA	ATACCTCGGGTTTCCACGTC
Collagen Type III, Alpha 1 Chain	Col3a1	CTGGTCCTGCTGGAAAGGAT	TCCATTGCGTCCATCAAAGC
Galectin-3	Gal3	GCTTATCCTGGCTCAACTGC	TTCACTGTGCCCATGATTGT
Growth/ Differentiation Factor 15	GDF15	GTCCAGAGGTGAGATTGGGG	CTTCAGGGGCCTAGTGATGTC
Interleukin 1 Receptor Like 1	ST2	GCAATTCTGACACTTCCCATG	ACGATTTACTGCCCTCCGTA

Table S3: Dobutamine stress echocardiography.

Parameter	Control	ISO	*p* value
Physiologic Data			
Heart Rate, bpm (Δ, %)	418 ± 25 (+13 ± 7)	399 ± 18 (+17 ± 7)	0.53 (0.73)
Parasternal Long-Axis View			
EF, % (Δ, %)	79 ± 4 (+73 ± 7)	78 ± 4 (+71 ± 11)	0.82 (0.88)
FAC, % (Δ, %)	60 ± 4 (+94 ± 11)	59 ± 4 (+97 ± 17)	0.81 (0.90)
EDV, µL (Δ, %)	44 ± 3 (-33 ± 7)	46 ± 2 (-32 ± 6)	0.66 (0.87)
ESV, µL (Δ, %)	10 ± 2 (-65 ± 11)	11 ± 2 (-60 ± 9)	0.79 (0.78)
Stroke Volume, µL (Δ, %)	34 ± 2 (+24 ± 6)	35 ± 2 (+21 ± 7)	0.76 (0.72)
Parasternal Short-Axis View			
$EF_{Teichholz}$, % (Δ, %)	88 ± 4 (+56 ± 8)	82 ± 2 (+56 ± 9)	0.19 (0.96)
FS, % (Δ, %)	58 ± 4 (+103 ± 15)	51 ± 3 (+90 ± 15)	0.12 (0.58)

EF: ejection fraction; $EF_{Teichholz}$: EF according to Teichholz formula; FAC: fractional area change; FS: fractional shortening; EDV: end-diastolic volume; ESV: end-systolic volume. *n*=7-11 per group; *Student's* t-test.

Table S4: Receiver operating characteristics.

Parameter	AUC (95% CI)	*p* value	Optimal cut off (unit)	Sensitivity (95% CI)	Specificity (95% CI)
GLS	0.93 (0.81-1.04)	**<0.0001**	-14.2 (%)	0.92 (0.62-1.00)	0.90 (0.56-1.00)
GLSR	0.78 (0.58-0.97)	**0.03**	-3.7 (1/s)	0.50 (0.21-0.79)	1.00 (0.69-1.00)
IVRT	0.85 (0.69-1.02)	**0.005**	20.6 (ms)	0.75 (0.43-0.95)	0.90 (0.56-1.00)
E/e'	0.87 (0.70-1.03)	**0.004**	39.3 (ratio)	0.92 (0.62-1.00)	0.80 (0.44-0.97)
MD_{Endo}	0.74 (0.51-0.97)	0.07	1.179 ($10^{-3}mm^2/s$)	1.00 (0.72-1.00)	0.45 (0.14-0.79)
$MD_{Transmural}$	0.73 (0.49-0.96)	0.09	1.112 ($10^{-3}mm^2/s$)	0.91 (0.59-1.00)	0.56 (0.21-0.86)
λ_{2Endo}	0.73 (0.50-0.96)	0.08	1.113 ($10^{-3}mm^2/s$)	0.73 (0.39-0.94)	0.78 (0.40-0.97)
HA_{Epi}	0.87 (0.71-1.03)	**0.006**	-16.55 (°degree)	0.82 (0.48-0.98)	0.89 (0.52-1.00)
$HA_{Transmural}$	0.84 (0.66-1.02)	**0.01**	4.05 (°degree)	0.82 (0.48-0.98)	0.78 (0.40-0.97)
pos./neg. HA_{Total}	0.81 (0.60-1.0)	**0.02**	1.14 (ratio)	0.73 (0.39-0.94)	0.89 (0.52-1.00)

AUC: Area under the ROC Curve; CI: Confidence Interval; GLS: Global Peak Longitudinal Strain; GLSR: Global Longitudinal Strain Rate; IVRT: Isovolumic Relaxation Time; MD_{Endo}: Subendocardial Mean Diffusivity; $MD_{Transmural}$: Transmural Mean Diffusivity; λ_{2Endo}: Subendocardial λ_2; HA_{Endo}: Subendocardial Helix Angle; $HA_{Transmural}$: Transmural Helix Angle; pos./neg. HA_{Total}: Ratio of Positive to Negative HA Values in the whole LV.

Supplemental Figures

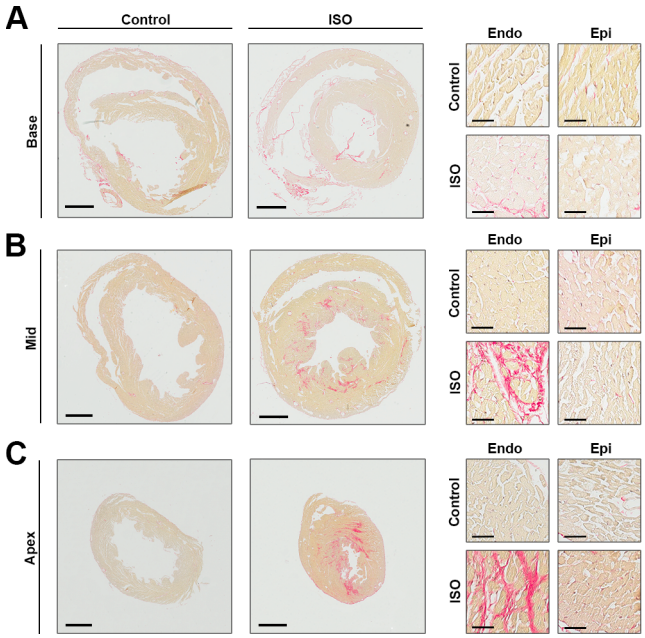

Figure S1: Segmental collagen quantification. (A) Representative cardiac cross-sections at basal level with magnified regions of interest within subendocardium and subepicardium. (B) Histologic analyses derived from mid-ventricular myocardium in the same arrangement as in A. (C) Histologic analyses derived from apical myocardium in the same arrangement as in A. (Picrosirius Red Staining; scale bars represent 1 mm and 40 µm, respectively).
Endo: subendocardium; Epi: subepicardium.

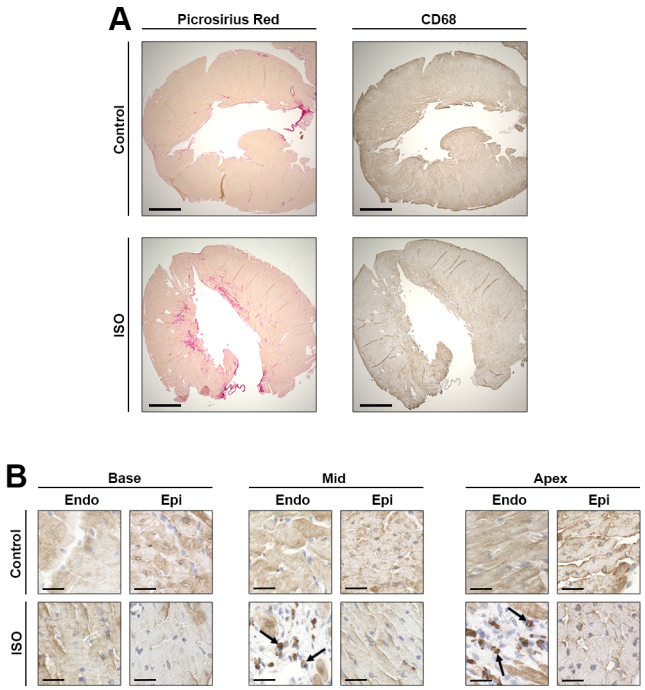

Figure S2: Immunhistochemical analysis. (A) Representative longitudinal sections of the heart stained for collagen (Picrosirius Red) and for the macrophage marker CD68 (scale bar: 1 mm). (B) Magnified regions of interest stained for CD68 in the different myocardial segments and layers (scale bar: 25 µm). Arrows indicate CD68-positive cells, which were predominantly located within fibrotic lesions in the mid-ventricular and apical subendocardium.
Endo: subendocardium; Epi: subepicardium.

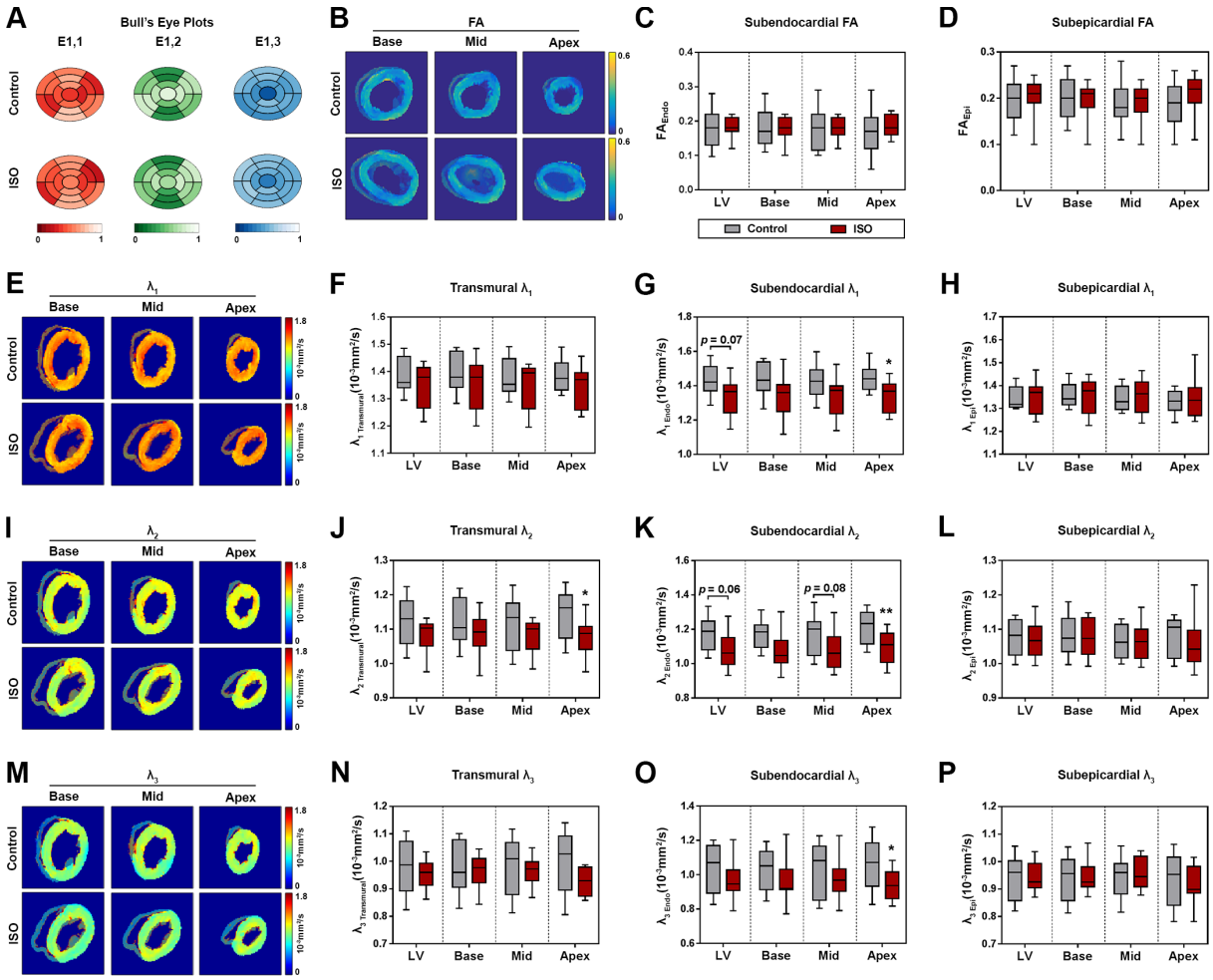

Figure S3: Diffusion metrics. (A) Representative bull's eye plots for all three vector components of the main eigenvector of diffusion derived from the 17-segment model. (B) Representative color maps for FA at different myocardial levels of animals treated with either saline (upper panel) or ISO (lower panel). (C) Subendocardial FA. (D) Subepicardial FA. (E) Representative color maps for λ_1 in the different myocardial segments of animals treated with either saline (upper panel) or ISO (lower panel). (F) Transmural λ_1. (G) Subendocardial λ_1. (H) Subepicardial λ_1. (I-L) Data for λ_2 presented in the same arrangement as in E-H. (M-P) Data for λ_3 presented in the same arrangement as in E-H.
E1,1-E1,3: Vector Components of the Main Eigenvector of Diffusion; Endo: Subendocardial; Epi: Subepicardial; λ_1-λ_3: Eigenvalues 1-3. *n*=9-11 per group; *Student's* t-test. **p*<0.05; ***p*<0.01.

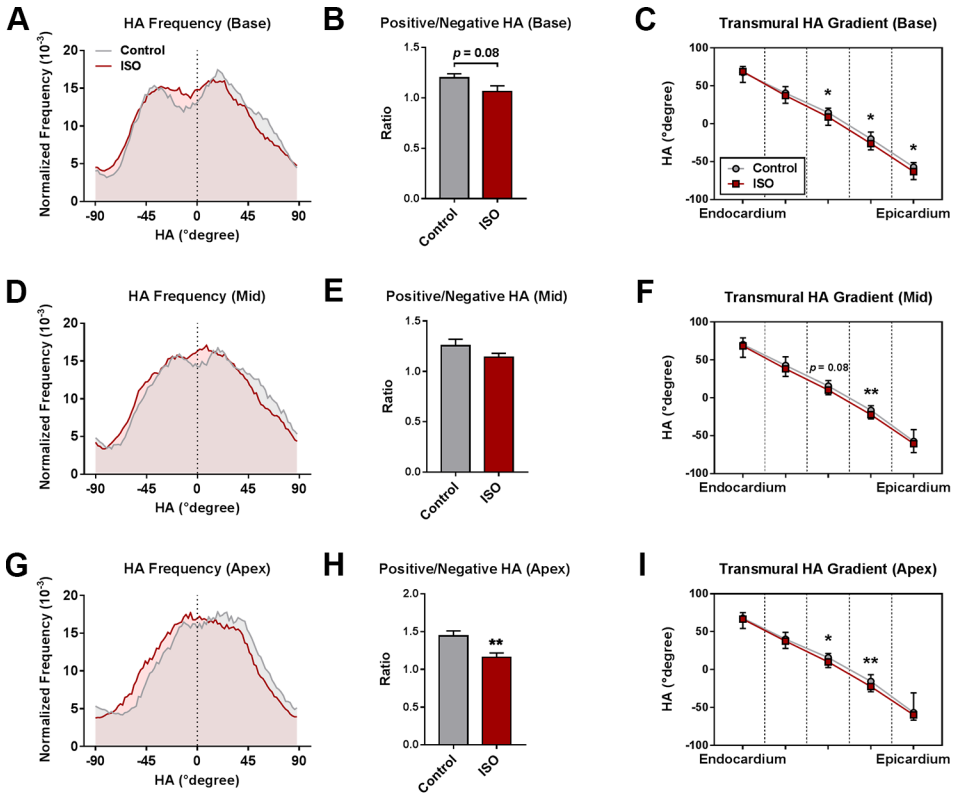

Figure S4: Microstructural changes in the different myocardial segments. (A) HA frequency in basal segments of the LV. (B) Ratio of positive to negative HA values in basal segments of the LV. (C) Transmural HA gradient in basal segments of the LV. (D-F) Data for mid-myocardial HA in the same arrangement as in A-C. (G-H) Data for apical HA in the same arrangement as in A-C.

n=9-11 per group; *Student's* t-test. **p*<0.05; ***p*<0.01.

A Novel Mono-surface Antisymmetric 8Tx/16Rx Coil Array for Parallel Transmit Cardiac MRI in Pigs at 7T

Ibrahim A. Elabyad, Maxim Terekhov, David Lohr, Maria R. Stefanescu, Steffen Baltes, and Laura M. Schreiber

Chair of Cellular and Molecular Imaging, Comprehensive Heart Failure Center (CHFC), University Hospital Wuerzburg, D-97078 Wuerzburg, Germany

Table S1. Simulated (yellow) and measured S-Matrix in dB for the mono-surface array loaded with a 20 cm diameter spherical phantom with ε_r = 59.3 and σ = 0.79 S/m.

El.#	1	2	3	4	5	6	7	8	9	10	11	12	13	14	15	16	El.#
	−12	−18	−16	−12	−21	−13	−25	−26	−22	−18	−27	−23	−24	−25	−26	−38	1
		−16	−16	−18	−16	−26	−17	−22	−16	−22	−24	−32	−21	−25	−33	−23	2
1	−10		−17	−18	−16	−26	−10	−26	−16	−22	−15	−28	−21	−25	−33	−27	3
2	−17	−10		−16	−24	−16	−37	−13	−22	−10	−31	−12	−29	−25	−34	−34	4
3	−18	−12	−14		−23	−20	−13	−27	−11	−27	−48	−26	−15	−42	−17	−40	5
4	−12	−18	−21	−14		−26	−26	−25	−28	−15	−42	−24	−27	−19	−30	−19	6
5	−20	−13	−16	−27	−21		−9.0	−35	−18	−30	−10	−30	−14	−27	−14	−28	7
6	−13	−20	−27	−16	−20	−21		−12	−32	−9.0	−47	−10	−30	−13	−29	−14	8
7	−24	−32	−12	−28	−16	−28	−21		−10	−30	−23	−29	−10	−31	−9.0	−35	9
8	−32	−24	−28	−12	−28	−16	−30	−22		−10	−40	−14	−43	−12	−37	−11	10
9	−19	−17	−9.0	−23	−15	−23	−11	−25	−15		−9.0	−31	−9.0	−31	−14	−28	11
10	−17	−19	−23	−9.0	−23	−15	−25	−11	−27	−15		−11	−34	−9.0	−40	−12	12
11	−22	−23	−15	−28	−19	−25	−8.0	−29	−16	−40	−17		−8.0	−33	−8.0	−41	13
12	−23	−22	−28	−15	−25	−19	−29	−8.0	−40	−16	−34	−17		−14	−44	−9.0	14
13	−22	−21	−24	−29	−25	−32	−12	−25	−10	−29	−8.0	−40	−15		−10	−31	15
14	−21	−22	−29	−25	−32	−25	−25	−12	−29	−10	−40	−8.0	−30	−15		−15	16
15	−27	−33	−19	−28	−18	−42	−10	−29	−8.0	−41	−20	−29	−8.0	−43	−22		
16	−33	−27	−28	−19	−43	−18	−29	−11	−41	−9.0	−29	−20	−43	−8.0	−39	−22	
	1	2	3	4	5	6	7	8	9	10	11	12	13	14	15	16	

Table S2. Measured S-Matrix in dB for the mono-surface array loaded with a 46 kg cadaver pig.

El.#	1	2	3	4	5	6	7	8	9	10	11	12	13	14	15	16
1	−17															
2	−13	−23														
3	−18	−12	−19													
4	−15	−20	−18	−15												
5	−19	−11	−13	−21	−28											
6	−11	−26	−24	−15	−19	−24										
7	−28	−15	−11	−37	−16	−33	−20									
8	−23	−25	−24	−13	−27	−21	−57	−18								
9	−22	−19	−23	−25	−12	−35	−21	−33	−15							
10	−20	−20	−18	−15	−35	−15	−30	−16	−28	−20						
11	−39	−26	−18	−52	−22	−30	−13	−40	−32	−33	−17					
12	−34	−37	−48	−20	−30	−40	−42	−13	−39	−20	−38	−27				
13	−31	−25	−36	−32	−21	−32	−16	−40	−15	−38	−12	−44	−25			
14	−26	−31	−26	−27	−35	−24	−40	−17	−37	−16	−36	−12	−44	−21		
15	−34	−40	−34	−47	−35	−38	−22	−45	−12	−43	−22	−52	−16	−48	−22	
16	−37	−30	−34	−37	−37	−22	−40	−19	−44	−13	−39	−17	−44	−12	−45	−22

Table S3. Computed optimal amplitudes/phases within the pig body phantom for the 8Tx channels after on-scanner pTx B_1^+ using the vendor integrated pTx shimming algorithm.

pTx Channel #	Magnitude	Phase [°]
T_{x1}	0.40	00.00
T_{x2}	0.41	33.68
T_{x3}	0.42	−98.95
T_{x4}	0.41	−41.85
T_{x5}	0.41	−12.14
T_{x6}	0.41	−69.62
T_{x7}	0.40	−33.25
T_{x8}	0.41	−19.95